Applied Catalysis B: Environmental 96 (2010) 486–495

Contents lists available at ScienceDirect

Applied Catalysis B: Environmental

journal homepage: www.elsevier.com/locate/apcatb

Effect of light source on the catalytic degradation of protocatechuic acid in a ferrioxalate-assisted photo-Fenton process

J.M. Monteagudo*, A. Durán, I. San Martín, M. Aguirre

University of Castilla-La Mancha, Grupo IMAES, Department of Chemical Engineering Escuela Técnica Superior de Ingenieros Industriales, Avda. Camilo José Cela, 1, 13071 Ciudad Real, Spain

ARTICLE INFO

Article history:
Received 18 January 2010
Received in revised form 25 February 2010
Accepted 3 March 2010
Available online 9 March 2010

Keywords:
Protocatechuic acid
Ferrioxalate
Photo-Fenton
UV light
CPC

ABSTRACT

The catalytic degradation of protocatechuic acid (PA) solutions in a ferrioxalate-assisted photo-Fenton process irradiated with solar or artificial ultraviolet light sources was investigated. The reactions were carried out either in a pilot plant consisting of a compound parabolic collector (CPC)-solar reactor or in a UV-A/C-lamp reactor. An optimization study was performed using a multivariate experimental design including the following variables: pH, temperature, solar power, air flow and initial concentrations of H_2O_2, Fe(II) and oxalic acid. The photocatalytic degradation efficiency was determined by measuring the elimination of the original PA and the removal of total organic carbon (TOC). TOC-removal rates of 97% and 96% were achieved under artificial UV-A/C and solar light, respectively, but with different optimum operating conditions. When artificial UV light was used in the presence of oxalic acid, the degradation rate was higher in the UV-C system than in the UV-A system because ferrioxalate complexes are primarily formed at 200–280 nm. •OH radicals were the main oxidative intermediate species in the artificial UV-A/C process while superoxide and •OH radicals played the most significant roles in the solar process. Artificial UV-A/C light can be used as an alternative to solar CPC on cloudy days.

1. Introduction

Agro-industrial wastewaters such as those produced in wine-making, olive-oil extraction or table-olive production contain significant concentrations of phenolic compounds, contributing to the toxicity of these effluents. It is well known that high concentrations of these compounds prevent mineralization of these effluents by conventional aerobic biological treatment processes [1,2]. Thus, there is currently considerable interest in developing alternative advanced oxidation processes (AOPs) for degrading these types of organic pollutants.

The homogeneous photo-Fenton reaction is one of the most effective systems for oxidation, generating mainly highly reactive hydroxyl radicals (•OH), as previously reported [3,4]. The application of solar irradiation to these systems could diminish the energy consumption required for generating hydroxyl radicals. The addition of oxalic acid to the photo-Fenton system promotes the formation of ferrioxalate complexes, which increases the oxidation efficiency of the solar photo-Fenton process, as ferrioxalate is a photo-sensitive complex which expands the useful range of the irradiation spectrum up to 550 nm [5,6], making the system a more cost-effective and environmentally benign treatment, as we reported previously [7].

A drawback of a solar system is that the reaction times are longer on cloudy days. This disadvantage could be solved if an artificially UV-irradiated pilot plant with both UV-C (for photolysis of H_2O_2) and UV-A (for ferrioxalate-complex photochemical reactions) lamps could be used in parallel on these days.

In this work, protocatechuic acid (PA) (Fig. 1a), typically found in agro-industrial wastes, was chosen as a model phenolic compound to evaluate the viability of their degradation under ferrioxalate-assisted artificial UV-A/C and solar photo-Fenton processes.

In recent years, ferrioxalate has been used in the photo-Fenton reaction involving ferric compounds [5,8–10], but there is very little information on the ferrioxalate-assisted photo-Fenton system using a ferrous-initiated process. The use of ferrous sulfate is advantageous since it is less corrosive than ferric salts, inexpensive and more soluble than ferric compounds. Additionally, Fe(II) is quickly converted into Fe(III) in the presence of hydrogen peroxide, so that the degradation of PA solutions is basically a process catalyzed by Fe(III)-oxalate.

The degradation of protocatechuic acid solutions has been studied previously using other advanced oxidation processes such as Fenton oxidation [11], photo-Fenton [12], O_3/UV or H_2O_2/UV methods [13]. However, the effect of ferrioxalate complexes on the degradation efficiency of PA using solar or artificial UV light sources

* Corresponding author. Tel.: +34 926295300x3888; fax: +34 926295361.
E-mail address: josemaria.monteagudo@uclm.es (J.M. Monteagudo).

0926-3373/$ – see front matter © 2010 Elsevier B.V. All rights reserved.
doi:10.1016/j.apcatb.2010.03.009

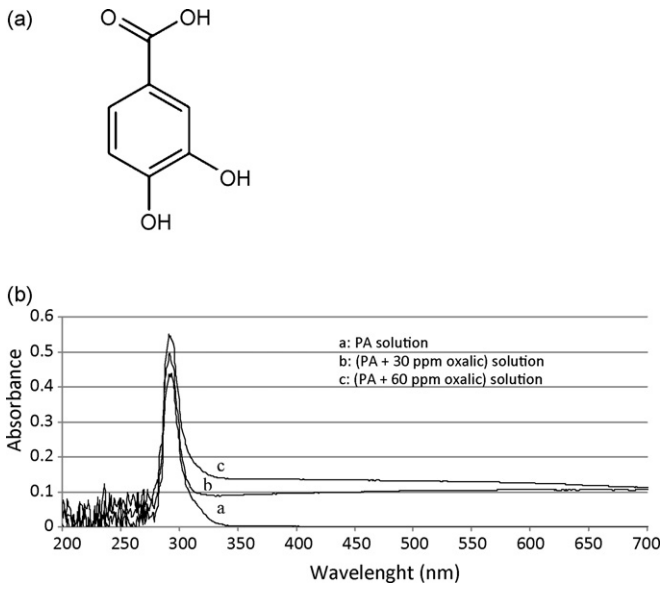

Fig. 1. (a) Protocatechuic acid (PA) chemical structure; (b) Effects of oxalic acid addition on absorption spectra of PA solutions.

has not been studied until now. In this work, a Multivariate Experimental Design according to the response-surface methodology [14] was performed to study the effect of all the variables simultaneously (pH, air-flow rate and initial concentrations of H_2O_2, Fe(II) and oxalic acid).

The experimental results were fitted using Neural Networks (NNs) [15,16], which allowed the values of kinetic degradation-rate constants (response functions) to be estimated within the studied range as a function of the process variables. Additionally, a saliency analysis of each variable in the NNs helped to discern their true relevance. As PA elimination does not necessarily imply total mineralization of the solution, the decrease of both PA and TOC concentrations were measured; residual H_2O_2, dissolved O_2 and Fe(II) concentrations were also determined. Finally, the contributions of different oxidative intermediate species to overall reaction were also quantified. The catalytic behavior of Fe and the effects of UV-A versus UV-C irradiation were also evaluated.

2. Experimental

2.1. Materials

Protocatechuic acid (3,4-dihydroxybenzoic acid) solutions were prepared by dissolving PA (Sigma–Aldrich, 97%) in distilled water without further purification. $FeSO_4{\cdot}7H_2O$ (Panreac, analytical grade) and $H_2C_2O_4{\cdot}2H_2O$ (Panreac, 99.5%) were added to the wastewater to form ferrioxalate complexes and used immediately in situ because of their light sensitivity. The initial concentration of PA was always 20 mg L^{-1}.

In all experiments, after the addition of Fe (II) and oxalic acid and pH adjustment, a measured amount of commercial hydrogen peroxide (30% (w/v), Merck) was added to the reactor to bring the H_2O_2 initial concentration to between 0 and 400 mg L^{-1}. The pH of the dye solutions was adjusted with 0.1 M H_2SO_4 and 6 M NaOH solutions as needed prior to degradation. To quantify the oxidation levels by radical reactions, the scavenging of free radicals was accomplished with 1,4-benzoquinone, NaN_3 and KI. Before analysis, all samples were withdrawn from the reactor and immediately treated with excess Na_2SO_3 solution to prevent further oxidation (this procedure was performed in order to prevent an overestimation of the degradation).

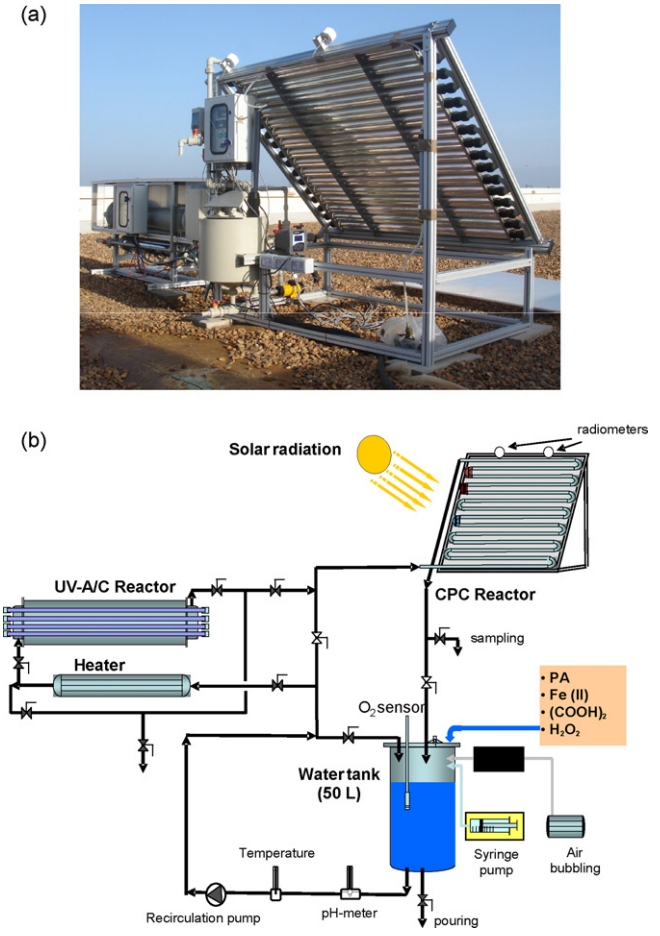

Fig. 2. Experimental setup based on a CPC and artificial UV-A/C pilot plants: (a) photo; (b) schematic.

2.2. Photochemical reactions

2.2.1. Solar-CPC pilot plant

The compound parabolic collector (CPC) pilot plant (manufactured by ECOSYSTEM, S.A.) comprises a solar reactor consisting of a continuously stirred tank (50 L), a centrifugal recirculation pump, and a solar collector unit with an area of 2 m^2 (concentration factor = 1). This unit was housed in an aluminum frame connecting the tubing and valves and mounted on a fixed south-facing platform tilted 39° (latitude of Ciudad Real, Spain) with respect to the horizontal plane (Fig. 2). The total illuminated volume inside the 16 borosilicate-glass absorber tubes was 16 L. UV irradiation was measured by a radiometer (Ecosystem, model ACADUS-85), which facilitated the measurement of the received irradiation as UV-A (300–400 nm). Data in terms of incident solar power (W m^{-2}) and accumulated solar energy (W h) were measured by means of a PLC (Programmable Logic Controller) coupled to the radiometer.

2.2.2. Artificial UV-A/C pilot plant

The UV pilot plant (FLUORACADUS-08/2.2, ECOSYSTEM, S.A.) is also shown in Fig. 2 and was composed of a 28-L reactor (2240 mm × 730 mm × 100 mm), with two UV-C lamps (200–280 nm; PHILIPS TUV TL D 55W HO SLV UV-C) and two UV-A lamps (320–400 nm; PHILIPS CLEO Effect 70W SLV). The UVC (for photolysis of H_2O_2) and UVA (for ferrioxalate-complex photochemical reactions) lamps were both used, either singly or simultaneously. This reactor was constructed of 7-mm-thick borosilicate and protected externally by a polypropylene tube. It accommodated four quartz tubes, 34 mm in diameter and 1.5 mm

Table 1
The 5-factor central composite design matrix. Ferrioxalate-assisted artificial UV-A/C and solar photo-Fenton systems.

Coded levels	Natural levels				
	$[H_2O_2]_o$ (mg L^{-1})	$[Fe(II)]_o$ (mg L^{-1})	$[H_2C_2O_4]_o$ (mg L^{-1})	Air flow (m^3 h^{-1})	pH
(+α)	400.00	20.00	60.00	1.60	6.00
(−α)	0.00	0.00	0.00	0.00	2.00
(+1)	284.09	14.20	42.61	1.14	4.84
(−1)	115.91	5.80	17.39	0.46	3.16
(0)	200.00	10.00	30.00	0.80	4.00
Response functions					
Solar process: $k_{PA\text{-}solar}$ (W^{-1} h^{-1}) and $k_{TOC\text{-}solar}$ (W^{-1} h^{-1})					
Artificial UV process: $k_{PA\text{-}UV}$ (min^{-1}) and $k_{TOC\text{-}UV}$ (min^{-1})					

	UV-A/C process	Solar process
Selected optimal conditions and best results obtained		
$[H_2O_2]_o$ (mg L^{-1})	125	320
$[Fe(II)]_o$ (mg L^{-1})	2	20
$[H_2C_2O_4]_o$ (mg L^{-1})	60	60
Air flow (m^3 h^{-1})	No air injection	No air injection
pH	4	4
k_{PA}	0.1405 min^{-1}	0.0493 W^{-1} h^{-1}
k_{TOC}	0.0542 min^{-1}	0.1759 W^{-1} h^{-1}
% PA elimination	100% (15 min)	100% (17 min)
%TOC removal	97% (210 min)	96% (180 min)

[protocatechuic acid] = 20 ppm.
Temperature typical range (°C): ≈22.0–32.5 °C.
Solar power typical range (W m^{-2}): ≈30–42 W m^{-2}.

thick, housing the lamps. For every reaction, the reservoir was charged with 50 L of PA solution and chemicals, and it was continuously pumped (flow rate: 30 L min^{-1}) into the UV-A/C reactor and afterwards into the CPC reactor. After flowing through all the tubes, the solution was recirculated back to the reservoir.

2.3. Analysis

Analysis of PA concentration was carried out by high-performance liquid chromatography with UV detection (HPLC-UV; Agilent Technologies 1100) in isocratic mode immediately after sampling. An Eclipse XDB-C18 column (5 μm, 4.6 mm × 250 mm) was used with an 18:82 (v/v) methanol/water mixture at acidic pH (2% acetic acid) as the mobile phase (detection wavelength, λ = 280 nm). Iron concentrations were obtained by photometric measurement with 1,10-phenanthroline according to ISO 6332 using a UV-Vis spectrophotometer (Zuzi 4418PC). The degree of mineralization was monitored by TOC variation determined with a TOC-5050 Shimazdu analyzer (standard deviation < 0.2 mg L^{-1}). The TOC contribution of the added oxalic acid had a relatively low significance as ferrioxalate is easily photolyzed, leading to the mineralization of oxalate. H_2O_2 in solution was determined by titration through an aqueous solution of potassium permanganate (0.02 M) using an automatic Titrino SET/MET 702 (Metrohm). Dissolved O_2 concentration was measured using a Lange LXV416 Luminescent Dissolved Oxygen (LDO) sensor.

2.4. Experimental design

Two central-composite experimental designs (CCED) consisting of 46 experiments each were applied to investigate the effects of five variables (initial concentrations of H_2O_2, Fe(II) and oxalic acid, pH and air-flow rate) in the ferrioxalate-assisted artificial UV-A/C or solar photo-Fenton process (Table 1; complete details of the CCED were as described previously [7]). Here, the initial concentration of PA (20 mg L^{-1}) was a constant and thus not considered as a factor. It is well known that an increase in the initial concentration of a contaminant compound decreases degradation efficiency because the path length of a photon entering the solution, and thus the amount of oxidative intermediate species generated, is decreased, so the probability of reaction is also decreased.

Each design consisted of three series of experiments [7]: (i) a 2^k factorial design (all possible combinations of the coded values +1 and −1), which in the case of $k = 5$ variables consisted of 32 experiments; (ii) axial or star points (coded values $\alpha = 2^{k/4} = \pm 2.378$) consisting of $2k = 10$ experiments; and (iii) replicates of the central point (4 experiments). Six additional experiments (three for the solar process and three for the artificial UV-A/C process) were carried out in the presence of radical-scavenging agents to complete the degradation study.

Incident solar power (in the solar process) and temperature (in both UV-A/C and solar processes) were not controlled during the experiment, but they were measured during the reaction and their average values were included in the fitting.

In all experiments, both the original PA elimination and the disappearance of TOC followed pseudo-first-order kinetics with respect to the PA and TOC concentrations, respectively, as follows:

$$r = -\frac{dC}{di} = kC \quad (1)$$

where r is the reaction rate, C is the concentration of PA or Total Organic Carbon (mg L^{-1}) at a given time i (min) (in the UV-A/C process) or at an accumulated solar energy i (W h) received by the water solution (in the solar process), k is the pseudo-first-order rate constant, namely, either $k_{PA\text{-}UV}$ or $k_{TOC\text{-}UV}$ (the PA-elimination-rate or mineralization-rate pseudo-constant, respectively, in the artificial UV process, min^{-1}) related to the reaction time, or $k_{PA\text{-}solar}$ or $k_{TOC\text{-}solar}$ (the PA elimination-rate or the mineralization-rate pseudo-constant, respectively, in the solar process, W^{-1} h^{-1}) related to the accumulated solar energy received by the water solution.

This equation can be integrated between $i = 0$ and $i = i$, yielding:

$$\ln \frac{C_0}{C} = ki \quad (2)$$

where C_0 is the initial concentration of PA or TOC. According to this expression, a plot of the first term versus i must yield a straight line satisfying Eq. (2) with slope k.

Table 2
Equations and parameters of Neural Network fittings for protocatechuic acid solutions degradation under the processes: ferrioxalate-assisted UV-A/C or Solar photo-Fenton.

Neural Network fitting

Equation[a] for PA elimination/Mineralization (artificial UV process)

$k_{PA\text{-}UV}/k_{TOC\text{-}UV}$ [min^{-1}] = $N_1 \times (1/(1 + 1/EXP([H_2O_2]_o \times W_{11} + [Fe]_o \times W_{12} + [pH] \times W_{13} + [H_2C_2O_4]_o \times W_{14} + [Temperature] \times W_{15} + [Air\ flow] \times W_{16}))) + N_2 \times (1/(1 + 1/exp([H_2O_2]_o \times W_{21} + [Fe]_o \times W_{22} + [pH] \times W_{23} + [H_2C_2O_4]_o \times W_{24} + + [Temperature] \times W_{25} + [Air\ flow] \times W_{26}$

Equation[a] for PA elimination/Mineralization (solar process)

$k_{PA\text{-}solar}/k_{TOC\text{-}solar}$ [$W^{-1}\ h^{-1}$] = $N_1 \times (1/(1 + 1/exp([H_2O_2]_o \times W_{11} + [Fe]_o \times W_{12} + [pH] \times W_{13} + [H_2C_2O_4]_o \times W_{14} + [Temperature] \times W_{15} + [Solar\ Power] \times W_{16} + [Air\ flow] \times W_{17}))) + N_2 \times (1/(1 + 1/EXP([H_2O_2]_o \times W_{21} + [Fe]_o \times W_{22} + [pH] \times W_{23} + [H_2C_2O_4]_o \times W_{24} + [Temperature] \times W_{25} + [Solar\ Power] \times W_{26} + [Air\ flow] \times W_{27})))$

Weight factors	Parameter	Values of neurons and factors to obtain k_{PA}		Values of neurons and factors to obtain k_{TOC}	
		UV process	Solar process	UV process	Solar process
N_1	**Neuron**	−0.8398	0.5686	0.0604	0.1244
W_{11}	$[H_2O_2]_o$	0.7692	−3.3961	1.0635	−2.4712
W_{12}	$[Fe(II)]_o$	−0.1254	2.0457	−0.0327	1.5996
W_{13}	pH	−3.8433	−0.4852	−4.5689	−0.5786
W_{14}	$[H_2C_2O_4]_o$	22.4343	0.4562	2.6453	0.7341
W_{15}	Temperature	−3.5056	−0.4861	1.6099	−0.5150
W_{16}	Solar power	–	1.8059	–	1.7259
W_{17}	Air flow	−3.1087	0.5508	0.6165	0.5400
N_2	**Neuron**	1.0855	−0.3202	−0.0472	−0.0646
W_{21}	$[H_2O_2]_o$	−0.5716	−30.404	1.9088	−12.7232
W_{22}	$[Fe(II)]_o$	0.0617	13.4512	0.0937	5.3229
W_{23}	pH	−0.9202	7.6703	6.6234	3.6283
W_{24}	$[H_2C_2O_4]_o$	7.4190	−9.1905	0.4845	−5.1059
W_{25}	Temperature	−0.9095	−20.3580	0.6357	−8.1274
W_{26}	Solar Power	–	24.8691	–	11.0575
W_{27}	Air flow	−3.1086	10.5078	0.8858	4.1391

Neural network output parameters	$[H_2O_2]_o$	$[Fe]_o$	pH	$[H_2C_2O_4]_o$	Temperature	Solar power	Air flow
Saliency analysis of the input variables for the neural network (%)							
$k_{PA\text{-}UV}$ (min^{-1})	3.24	0.41	8.76	59.02	8.26	–	20.30
$k_{TOC\text{-}UV}$ (min^{-1})	14.02	0.60	52.82	14.83	10.63	–	7.09
$k_{PA\text{-}solar}$ ($W^{-1}\ h^{-1}$)	31.46	16.86	5.92	6.42	11.38	20.46	7.50
$k_{TOC\text{-}solar}$ ($W^{-1}\ h^{-1}$)	27.83	15.11	7.16	9.59	11.26	21.60	7.44

[a] Parameters values in equations must be previously normalized to the (0.1) interval.

2.5. Neural network strategy

In this work, a linear basis function was used (a linear combination of inputs, X_j, and weight factors, W_{ij}; Table 2). Each neural network was solved with two neurons and used a simple exponential activation function [15,16]. The strategy was based on a back-propagation calculation. Parameters were found using the Solver tool in Excel using the Marquardt non-linear fitting algorithm [17]. Further details can be found in our previous report [7]. Finally, a measure of the saliency of the input variables was made based on the connection weights of the NNs. This allowed for analysis of the relevance of each variable with respect to the others (expressed as a percentage).

3. Results and discussion

3.1. Previous studies

Table 3 shows the results of an initial comparative study on the degradation of protocatechuic acid solutions in different sys-

Table 3
Protocatechuic acid degradation. A previous comparative study.

System	PA elimination (%)	TOC removal (%)
Solar	11.78	14.34
UV-A/C	20.59	15.26
Solar/UV-A/C	18.60	15.53
H_2O_2	0.00	0.00
UV-A/C/Fe(II)	13.62	12.86
UV-A/C/H_2O_2	88.53	48.88
UV-A/C/oxalic	48.00	4.99
H_2O_2/Fe	7.92	10.56
H_2O_2/Fe/oxalic	21.00	22.00
UV-A/C/H_2O_2/Fe(II)	85.00 (30 min); 100.00 (60 min)	71.38
Solar/H_2O_2/Fe(II)	88.00 (30 min); 100.00 (60 min)	61.20
UV-A/C/H_2O_2/Fe(II)/oxalic	100.00 (20 min)	80.00 (40 min)
UV-A/H_2O_2/Fe(II)/oxalic	84.00 (20 min); 100.00 (40 min)	57.00 (40 min)
UV-C/H_2O_2/Fe(II)/oxalic	88.00 (20 min); 100.00 (30 min)	70.00 (40 min)
Solar/H_2O_2/Fe(II)/oxalic	100.00 (15 Wh; 18 min)[a]	81.00 (60 Wh; 44 min)[b]

Experimental conditions: $[H_2O_2]$ = 100 ppm; [Fe(II)] = 2 ppm; [oxalic] = 60 ppm; pH = 4.

[a] 15 Wh accumulated solar energy; 18 min reaction time.

[b] 60 Wh accumulated solar energy; 44 min reaction time.

36 W m^{-2} Average solar power.

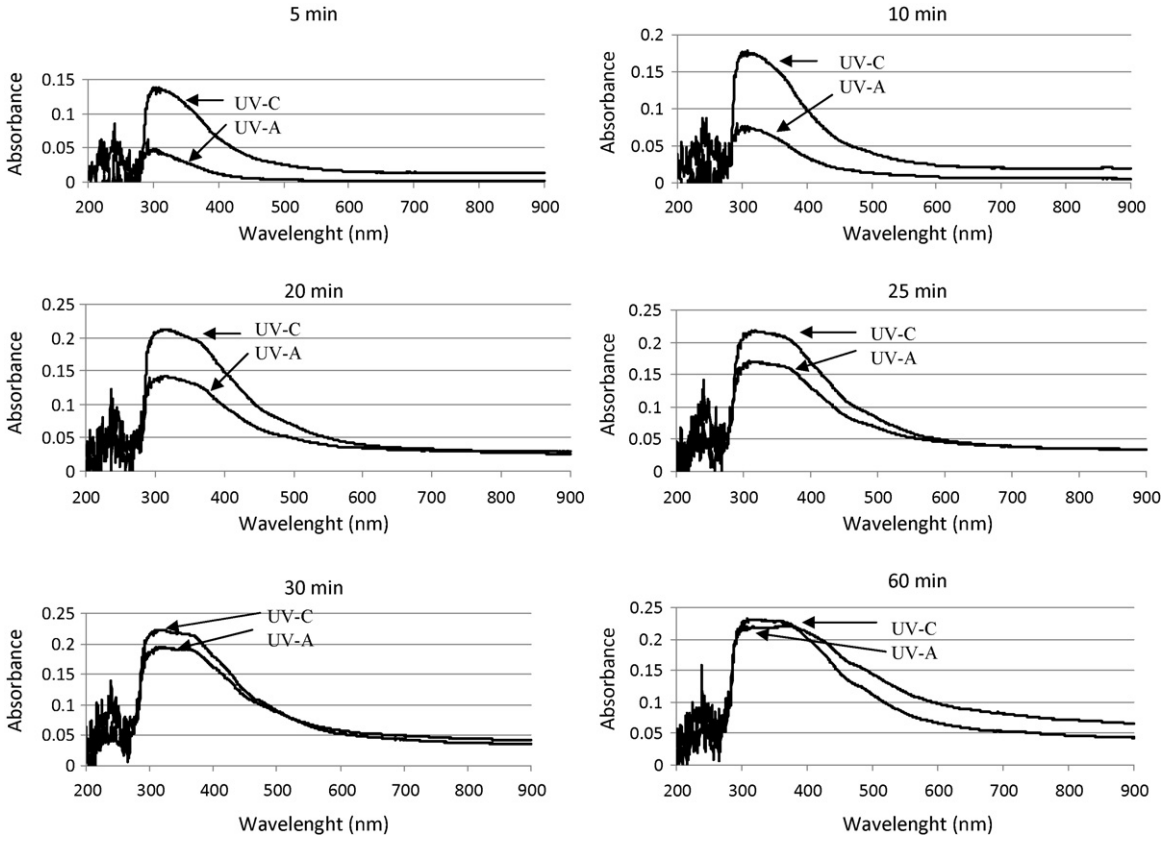

Fig. 3. Absorption spectra of (Fe(II)/oxalic) solutions irradiated by artificial UV-C or UV-A light as a function of time.

tems. Both target-compound elimination and mineralization of PA solutions via direct photolysis using single or combined solar and artificial UV-A/C light were very inefficient (<20%). The results also confirmed the negligible effect of H_2O_2 as a single oxidant, as direct reaction of peroxide with PA molecules does not occur. The use of artificial UV-A/C light in the presence of only Fe(II) did not improve the PA (13.62%) and TOC (12.86%) removal due to the fact that oxidative intermediate species (mainly hydroxyl radicals) are not generated under irradiation of ferrous ions in the absence of H_2O_2 or oxalic acid. When the PA solution was irradiated with UV-A/C light in the presence of H_2O_2 alone, the removal rates of PA and TOC were increased to 88.53% and 48.88%, respectively. In this case, as is well-known, hydroxyl radicals were generated by 200–300 nm photolysis of hydrogen peroxide, which indicates the favorable synergistic effect of hydrogen peroxide and UV-C light. Although $^{\bullet}OH$ radicals are produced in this system, their concentration was not sufficient to achieve total degradation of the PA solution. When the degradation reaction was carried out under UV-A/C light irradiation and oxalic acid added alone, original PA removal was increased from approximately 20 to 48% as compared with the single UV-A/C system. This could be due to the formation of PA-oxalate complexes which absorb more radiation and thus break down the aromatic ring of the target molecule. This effect is evident in Fig. 1b, showing the three absorption spectra of single PA solutions and of the compound plus 30 or 60 ppm of oxalic acid. However, the degree of mineralization was not increased because hydroxyl radicals were not generated, and TOC removal was lower than 5%, indicating that intermediate compounds possibly more difficult to break down are formed. The treatment with Fenton reagent (H_2O_2 + Fe(II)) alone or oxalic-assisted Fenton reagent increased the degradation efficiency compared to the system using H_2O_2 alone, as expected. All the other systems studied used Fenton reagent with solar or artificial UV light in the presence or absence of oxalic acid, and they all led to 100% PA elimination, although with different reaction rates depending on operating conditions. In these prior experiments, the maximum TOC removal efficiency (80–81%) was obtained with the ferrioxalate-assisted UV-A/C or solar photo-Fenton systems. The increased degradation efficiency could be due to the continuous regeneration of Fe^{2+} via photo-reduction of Fe^{3+} with 200–400 nm UV light and extra generation of free radicals (mainly $^{\bullet}OH$) by H_2O_2 photolysis or ferrioxalate photochemistry [7]. The results of degradation using UV-A (320–400 nm) lamps or UV-C (200–280 nm) lamps alone in the H_2O_2/Fe(II)/oxalic system revealed that photolysis of H_2O_2 (under UV-C) plays a more significant role than ferrioxalate photochemistry (under UV-A) in the generation of oxidative intermediate species. However, the results shown in Fig. 3 could also justify these results. Here, the absorption spectra of (Fe(II) + oxalic) solutions irradiated by UV-C or UV-A light as a function of time show that the formation of ferrioxalate complexes is more rapid when UV-C is used. This is possibly due to the quicker photo-reduction of Fe(III) into Fe(II) according to Eq. (3) at approximately 320 nm. These Fe(III) ions are formed by the oxidation of ferrous iron (added as $FeSO_4$) by dissolved oxygen (Eq. (4)). Thus, the available amount of Fe(III) to form ferrioxalate complexes is higher in the UV-C system. After 60 min, both spectra were similar, but ferrioxalate photochemistry, generating extra free radicals, first began when the solution was irradiated by UV-C light. As shown, the total elimination of target compound takes place in 30 or 40 min using UV-C or UV-A light, respectively (Fig. 3). However, the TOC removal at 40 min was much higher in the UV-C system (70%) than in the UV-A process (57%).

$$Fe(III)(OH)^{2+} + h\nu \rightarrow Fe(II) + {}^{\bullet}OH \quad (3)$$

$$Fe(II) + O_2 \rightarrow Fe(III) + O_2^{\bullet -} \quad (4)$$

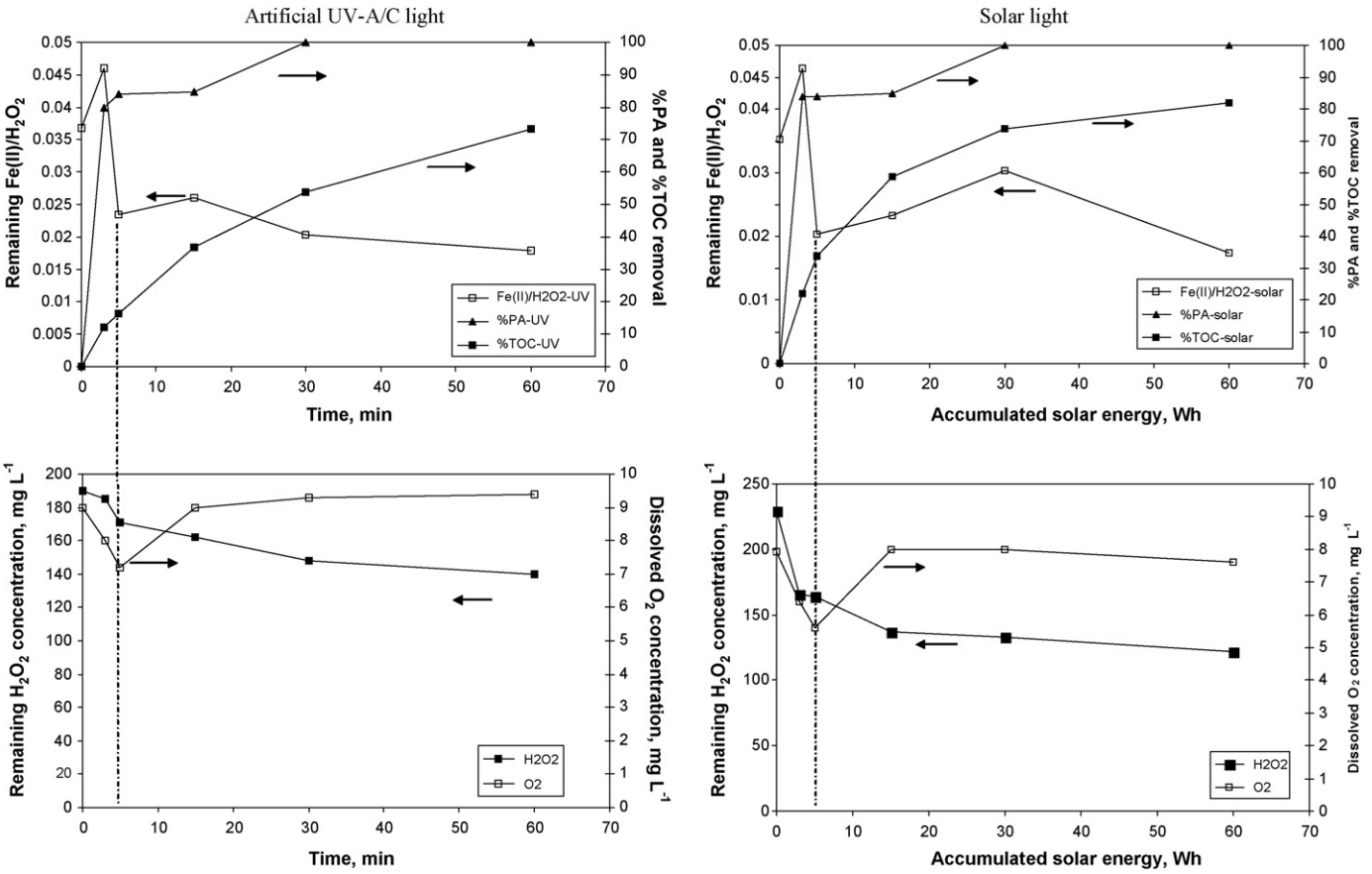

Fig. 4. Protocatechuic acid elimination and mineralization of PA solutions in the ferrioxalate-assisted UV-A/C or solar photo-Fenton systems; evolution of Fe(II)/H_2O_2 molar ratio and remaining concentrations of peroxide and dissolved oxygen. Experimental conditions: $[H_2O_2]$ = 200 mg L^{-1}; [Fe(II)] = 20 mg L^{-1}; $[H_2C_2O_4]$ = 30 mg L^{-1}; pH = 4; [PA] = 20 mg L^{-1}, air-flow rate = 0.8 Nm^3 h^{-1}. Average temperature: 30 °C. Average solar power: 40 W m^{-2}.

Taking into account the results from this previous study, two central-composite experimental designs were applied to optimize the ferrioxalate-assisted photo-Fenton processes under two light sources: (1) solar light, as this solar-activated catalytic system could offer an economical and practical alternative for the destruction of this type of contaminant; and (2) artificial UV-A/C light, which could be used on cloudy days.

3.2. Artificial UV-A/C and solar pilot plants

All the experiments presented in this section were based on the degradation of protocatechuic acid solutions in a ferrioxalate-assisted photo-Fenton system irradiated under artificial UV-A/C or solar light. In all of these, both the disappearance of the target compound and total organic carbon removal followed pseudo-first-order kinetics with respect to the PA and TOC concentrations, respectively, as indicated above. To study the effect of the variables pH, air-flow rate and initial concentrations of H_2O_2, Fe(II) and oxalic acid on the response functions ($k_{PA\text{-}solar}$, $k_{PA\text{-}UV}$, $k_{TOC\text{-}solar}$ and $k_{TOC\text{-}UV}$) two central-composite designs were utilized; the experimental design matrix, coded and natural levels, and variable ranges are presented in Table 1, which also shows the selected optimal operating conditions for each process as well as the best results obtained for k_{PA}, k_{TOC} and PA elimination and TOC removal percentages. Solar power (in the solar process) and temperature (in both systems) were not controlled during the experiment, but they were measured during the reaction and their average values were included in the fitting.

Experimental results and NN predictions of these constants were in good agreement, with an average error lower than 15% in all cases (data not shown). The equation and fitting parameters for k_{PA} and k_{TOC} are shown in Table 2. N_1 and N_2 are general factors related to the first and the second neuron, respectively. W_{11} to W_{16} (UV-light process) and W_{11} to W_{17} (solar process) are the contribution parameters to the first neuron and represent the influence of each of the variables in the process ($[H_2O_2]$, [Fe(II)], $[H_2C_2O_4]$, pH, air-flow rate, average temperature and average incident solar power (in the case of the solar light system); W_{21} to W_{26} (artificial UV process) and W_{21} to W_{27} (solar process) are the contributions to the second neuron corresponding to the same variables.

The results of a saliency analysis on the input variables for each neural network are also shown in Table 2. From these results, it was possible to deduce the effects of each parameter on the studied variables, reported as percentages. It was confirmed that over the studied range in the artificial UV-A/C process, the initial concentration of oxalic and pH were the most significant factors affecting the PA elimination and mineralization, respectively. In the solar process, the initial concentration of H_2O_2 had a more significant influence on both PA elimination and solution mineralization rates.

3.2.1. Reaction analysis

As an example, Fig. 4 shows a comparative analysis of the degradation of PA solutions in the two ferrioxalate-assisted photo-Fenton systems using artificial UV-A/C and solar light sources. The experimental conditions used are shown in Fig. 4, although the variation of the studied parameters was reproducible in all experiments. As can be seen, during the reaction the evolution of the parameters (molar ratio of remaining Fe(II)/H_2O_2, %PA elimination, %TOC removal, remaining H_2O_2 and dissolved oxygen concentration) was similar in both systems. In the first stage of the reaction, in

less than 4 min (UV process) or 4 W h of accumulated solar energy (solar process; ≈4 min in this case) elimination of approximately 85% of the original PA was achieved. However, the mineralization degree was only between 15 and 20% for both systems, indicating that protocatechuic acid rapidly oxidized into intermediates. After 30 min (30 W h in the solar process) of reaction, 100% of the PA initial was removed. At that time, 75% and 58% TOC removals were attained in the solar and artificial UV-A/C processes, respectively. During this first stage, H_2O_2 concentration rapidly decreased, followed by a second, slower, depletion stage. The consumption of H_2O_2 could be due to any of the following reactions:

$$Fe(II) + H_2O_2 \rightarrow Fe(III) + OH^- + {}^{\bullet}OH \quad (5)$$

$$H_2O_2 \rightarrow O_2 + H_2O \quad (6)$$

$$H_2O_2 + {}^{\bullet}OH \rightarrow HO_2{}^{\bullet} + H_2O \quad (7)$$

$$Fe(III) + H_2O_2 \rightarrow Fe(II) + O_2 + 2H_2O \quad (8)$$

$$H_2O_2 + HO_2{}^{\bullet} \rightarrow O_2{}^{\bullet} + {}^{\bullet}OH + H_2O \quad (9)$$

Additionally, when ferrioxalate complex $[Fe(III)(C_2O_4)_3]^{3-}$ is irradiated from the ultraviolet to the visible range in the presence of H_2O_2, reactions (10) to (13) take place, with H_2O_2 also being consumed by Eq. (13):

$$Fe(III)[(C_2O_4)_3]^{3-} + h\nu \rightarrow Fe(II) + 2C_2O_4{}^{2-} + C_2O_4{}^{\bullet-} \quad (10)$$

The oxalyl radical anion, $C_2O_4{}^{\bullet-}$, quickly decomposes to the carbon dioxide radical anion, $CO_2{}^{\bullet-}$:

$$C_2O_4{}^{\bullet-} \rightarrow CO_2{}^{\bullet-} + CO_2 \quad (11)$$

This reducing agent can produce Fe(II) via reaction (12):

$$CO_2{}^{\bullet-} + Fe(III)[(C_2O_4)_3]^{3-} \rightarrow Fe(II) + CO_2 + 3C_2O_4{}^{2-} \quad (12)$$

When ferrioxalate is irradiated in the presence of H_2O_2, one $^{\bullet}OH$ for every Fe(II) is generated:

$$Fe(II) + H_2O_2 + C_2O_4{}^{2-} \rightarrow Fe(III)[(C_2O_4)_3]^{3-} + OH^- + {}^{\bullet}OH \quad (13)$$

In this initial stage of the reaction, the dissolved O_2 concentration rapidly decreased until a minimum value was reached and then increased until a plateau value was achieved, which indicates the less significant role of O_2 during the mineralization stage. The decrease of dissolved O_2 could be due to the reaction of oxygen with the oxalyl radical anion, $C_2O_4{}^{\bullet-}$, according to Eq. (14) and with intermediate organoradicals by Eq. (15), in agreement with other researchers [18,19]. After this period, the dissolved oxygen concentration increased, likely due to ferrioxalate photochemistry reactions (Eqs. (10), (16), (17) and (18)), by H_2O_2 decomposition (Eq. (6)) and by catalytic reactions of Fe(III) with either H_2O_2 or $HO_2{}^{\bullet}$ according to Eqs. (8) and (19), respectively. Both oxygen depletion and formation reactions occur throughout the process. Depending on the availability of the reagents and some other factors, one of the reactions becomes dominant at different stages of the reaction.

$$C_2O_4{}^{\bullet-} + O_2 \rightarrow O_2{}^{\bullet-} + 2CO_2 \quad (14)$$

$$R^{\bullet} + O_2 \rightarrow RO_2{}^{\bullet} + H_2O \rightarrow ROH + HO_2{}^{\bullet} \quad (15)$$

$$C_2O_4{}^{\bullet-} + [Fe(C_2O_4)_3]^{3-} \rightarrow Fe(II) + 3C_2O_4{}^{2-} + 2CO_2 \quad (16)$$

$$O_2{}^{\bullet-} + H^+ \rightarrow HO_2{}^{\bullet} \quad (17)$$

$$HO_2{}^{\bullet} + HO_2{}^{\bullet} \rightarrow H_2O_2 + O_2 \quad (18)$$

$$Fe(III) + HO_2{}^{\bullet} \rightarrow Fe(II) + O_2 + H^+ \quad (19)$$

In contrast, the Fe(II)/H_2O_2 molar ratio increased because of the high hydrogen peroxide consumption until a maximum value was achieved and then dropped until a minimum value was reached. At that time, the dissolved oxygen concentration began to increase.

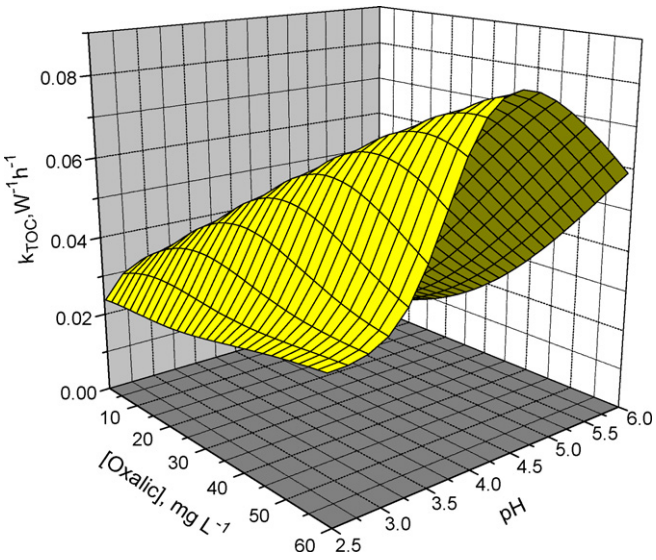

Fig. 5. Mineralization of protocatechuic acid solutions in the ferrioxalate-assisted solar Photo-Fenton process; effects of pH and oxalic acid dose. $[H_2O_2] = 200\ mg\ L^{-1}$; $[Fe(II)] = 10\ mg\ L^{-1}$; $[PA] = 20\ mg\ L^{-1}$; air-flow rate = 0.8 $Nm^3\ h^{-1}$. Average temperature: 25 °C; Average solar power: 35 W m^{-2}.

Regarding mineralization of the solutions, the TOC degradation rate slowed down at the end of the reaction, indicating the formation of difficult-to-degrade intermediates. It would be of interest to further study the character of such by-products formed during the reaction, but it was outside the scope of this work, which only attempted to demonstrate the mineralization of PA solutions in the ferrioxalate-catalyzed artificial UV/solar system in the presence of H_2O_2. An interesting point is that the mineralization was more rapid under solar irradiation. This could be due to the significant absorbance of PA between 280 and 310 nm (Fig. 1b) and, therefore, the formation of its possible reaction intermediates as well. Thus, a quenching effect could be produced by PA and its intermediates in the wavelength range of the UV-A/C system (200–400 nm). As the ferrioxalate photochemistry makes use of light up to 550 nm, a major part of the solar radiation capable of inducing reaction was not affected by this quenching effect and the TOC removal rate was higher.

3.3. Effect of pH and oxalic acid addition

Fig. 5 shows (as an example) the effect of pH and the addition of oxalic acid on the value of the mineralization rate constant, $k_{TOC\text{-}solar}$, as simulated by the NNs (using the equation shown in Table 2; operating conditions: $[H_2O_2] = 100\ mg\ L^{-1}$; $[Fe(II)] = 2\ mg\ L^{-1}$; $[H_2C_2O_4] = 60\ mg\ L^{-1}$; pH 4; $[PA] = 20\ mg\ L^{-1}$; average temperature: 25 °C; average solar power = 35 W m^{-2}). The results revealed that varying the pH and the addition of oxalic acid to the Fe(II)/H_2O_2 system irradiated with sunlight could increase the reaction rate or cause inhibition effects depending on the operating conditions. Thus, if the reaction was conducted at pH values below approximately 4, the initial concentration of oxalic acid positively affected the photocatalytic reaction until an optimal value was used, and this optimal value increased as the pH increased. This was due to the faster generation of Fe^{2+} ion by photolysis of ferrioxalate and additional hydroxyl radicals produced at that optimal pH value near 4. Fe(II) may react by Eqs. (5) and (13) generating more $^{\bullet}OH$ radicals. An excess of oxalic acid cannot complex with ferric ions in solution and the light penetration through irradiated wastewater decreases. Above pH 4–4.5, the influence of oxalic acid was positive over the studied range (between 0 and 60 $mg\ L^{-1}$).

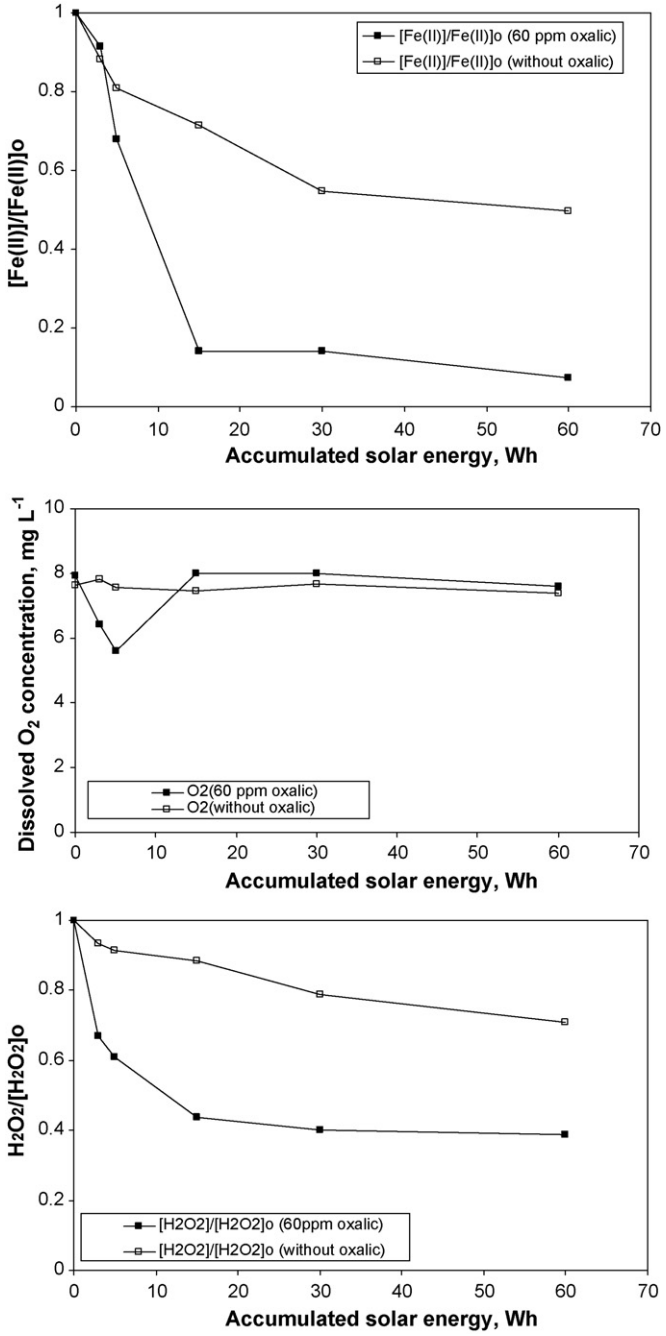

Fig. 6. Effect of the presence of oxalic acid on remaining Fe(II), dissolved O_2 concentration, and H_2O_2 conversion during the degradation of protocatechuic acid solutions in the ferrioxalate-assisted solar photo-Fenton process. Experimental conditions: $[H_2O_2] = 200\ mg\ L^{-1}$; $[Fe(II)] = 10\ mg\ L^{-1}$; $[H_2C_2O_4] = 60\ mg\ L^{-1}$; air-flow rate: $0.8\ Nm^3\ h^{-1}$; pH = 4; [PA] = $20\ mg\ L^{-1}$; Average temperature: 30 °C; Average solar power: $31\ W\ m^{-2}$.

When the pH was greater than 4.5, the process efficiency decreased, as the coagulation of Fe(III) complexes reduces the catalyst effect of Fe(II) to decompose H_2O_2, as we reported previously [7].

Fig. 6 shows the evolution of remaining Fe(II), dissolved oxygen concentration and H_2O_2 conversion during the degradation reaction of PA solutions in the solar photo-Fenton process at pH 4 in the absence or presence of $60\ mg\ L^{-1}$ oxalic acid. Here, the conversion of Fe(II) and H_2O_2 was higher when oxalic acid was added, the ferrioxalate photochemistry being more active. In these conditions, oxygen played the most important role in the degradation reactions in the presence of ferrioxalate, as indicated above.

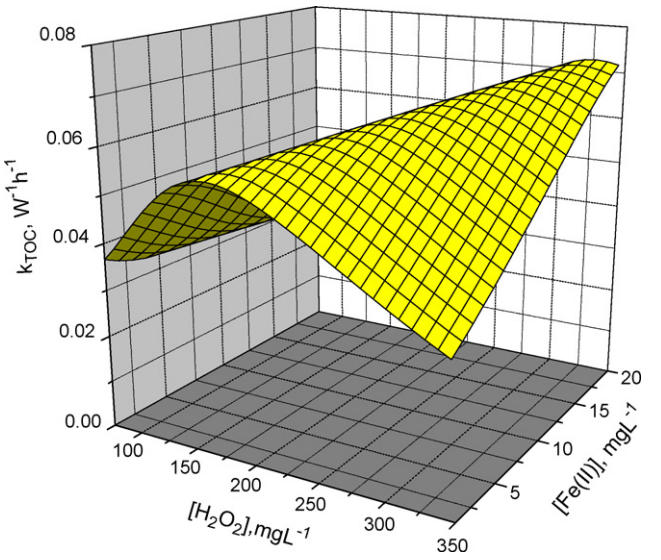

Fig. 7. Mineralization of protocatechuic acid solutions in the ferrioxalate-assisted solar Photo-Fenton process; effects of initial concentrations of Fe(II) and H_2O_2. $[H_2C_2O_4] = 30\ mg\ L^{-1}$; pH = 4; [PA] = $20\ mg\ L^{-1}$; air-flow rate = $0.8\ Nm^3\ h^{-1}$; Average temperature: 25 °C; Average solar power: $35\ W\ m^{-2}$.

3.4. Effect of the initial concentrations of Fe(II) and H_2O_2

Fig. 7 shows (as an example) the mineralization rate constants of PA solutions in the ferrioxalate-assisted solar photo-Fenton process. At a constant initial ferrous concentration, $k_{TOC\text{-}solar}$ increased with initial H_2O_2 concentration over the studied range until an optimal concentration of hydrogen peroxide was used. This fact indicates that Fe^{2+} can significantly accelerate the decomposition of H_2O_2 to form more hydroxyl radicals. Above this optimal hydrogen peroxide concentration, a decrease of $k_{TOC\text{-}solar}$ was observed. It is well known that an increase in H_2O_2 concentration produces a higher amount of •OH radicals. However, an excess of hydrogen peroxide reduces catalytic activity, reducing the amount of radicals available and producing the well-known *scavenger effect*. Although other radicals (e.g., $HO_2^{\bullet}$) are produced, their oxidation potential is much smaller than that of the hydroxyl radicals. Additionally, decomposition of hydrogen peroxide to form water and oxygen is also favored. This optimal value of H_2O_2 increased as the initial concentration of Fe(II) increased. The hydrogen peroxide decomposition reaction and ferrioxalate photochemistry are favored when the initial Fe(II) concentration is increased, as expected. When the initial concentration of H_2O_2 was smaller than optimal, an increase of Fe(II) negatively affected k_{TOC} because an inhibition effect was present, possibly due to the excess Fe(II) competing with PA molecules for various radicals, as shown in Eqs. (20) to (22):

$$Fe(II) + {}^{\bullet}OH \rightarrow Fe(III) + OH^{-} \quad (20)$$

$$Fe(II) + HO_2^{\bullet} \rightarrow Fe^{(III)}(HO_2)^{2+} \quad (21)$$

$$Fe(II) + O_2^{\bullet -} + H^{+} \rightarrow Fe^{(III)}(HO_2)^{2+} \quad (22)$$

3.5. Degradation mechanism

Several additional different comparative experiments were carried out to determine the main active species responsible for the mineralization of PA solutions depending of the nature of the radiation. In these reactions, various oxidative intermediate species can be generated such as hydroxyl radical (•OH), hydroperoxyl ($HO_2^{\bullet}$), singlet oxygen ($^1O_2$) and superoxide radical anion ($O_2^{\bullet -}$). Thus, the degradation process was developed in the absence and in the presence of appropriate quenchers of these species [20] under

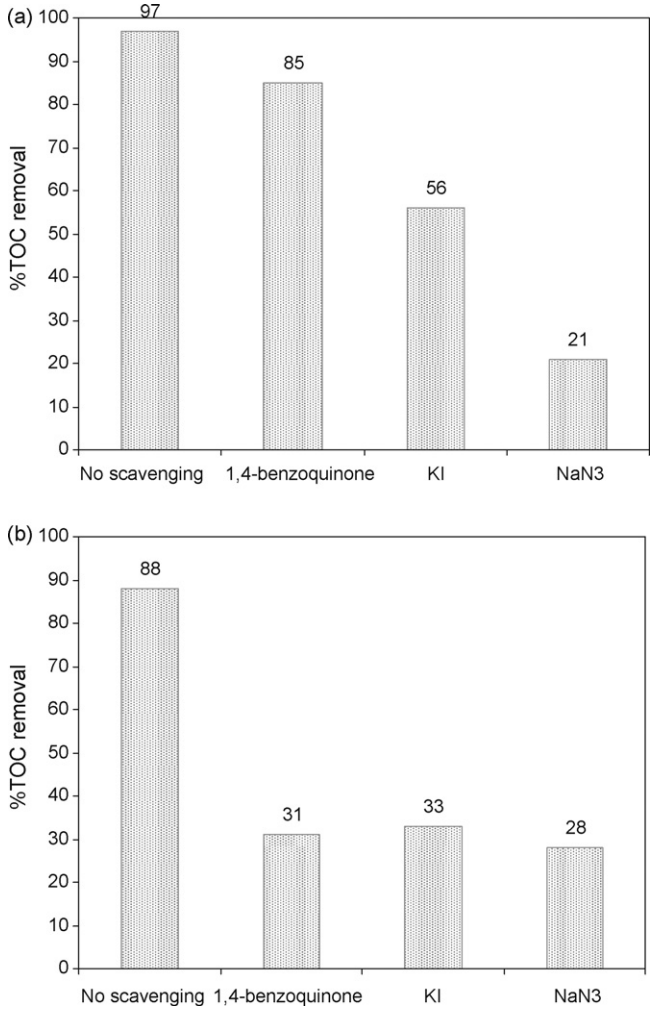

Fig. 8. Mineralization of protocatechuic acid solutions in the ferrioxalate-assisted UV-A/C (a) and solar (b) photo-Fenton process in the presence of 2 mM scavenging agents 1,4-benzoquinone, KI and NaN_3. Experimental conditions: $[H_2O_2] = 100\ mg\ L^{-1}$; $[Fe(II)] = 2\ mg\ L^{-1}$; $[H_2C_2O_4] = 60\ mg\ L^{-1}$; pH = 4; $[PA] = 20\ mg\ L^{-1}$. (a) Artificial UV-A/C process; (b) solar process.

the same conditions. The scavenging agents used were the following: 1,4-benzoquinone ($C_6H_4O_2$, a quencher of superoxide radical anion), sodium azide (NaN_3, a quencher of singlet oxygen which may also interact with hydroxyl radicals) and potassium iodide (KI, a quencher of hydroxyl radicals). Fig. 8a illustrates that, under artificial UV-A/C light, the addition of 1,4-benzoquinone slightly affected %TOC removal, reducing the degree of mineralization from 97 to 85%, indicating that $O_2^{\bullet -}$ was not an important oxidative intermediate species. The values of %TOC removal in the presence of NaN_3 and KI indicated that $^{\bullet}OH$ radicals were the main oxidative intermediate species, with KI reducing the degree of mineralization from 97 to 56%. Singlet oxygen can be formed when oxygen molecules absorb photons and are activated [21]. Singlet oxygen also played an important role; the addition of NaN3 reducing the degree of TOC removal due to $^1O_2$ from 56 to 21%. When $^{\bullet}OH$ and $^1O_2$ were scavenged by NaN_3, the mineralization of PA solutions was by the action of superoxide radicals ($O_2^{\bullet -}$) produced in the reaction between oxygen and the carbon dioxide radical anion formed by ferrioxalate photochemistry:

$$CO_2^{\bullet -} + O_2 \rightarrow O_2^{\bullet -} + CO_2 \quad (23)$$

In this case, the degradation efficiency was lower because, at acid pH, an amount of superoxide radicals is transformed into $HO_2^{\bullet}$

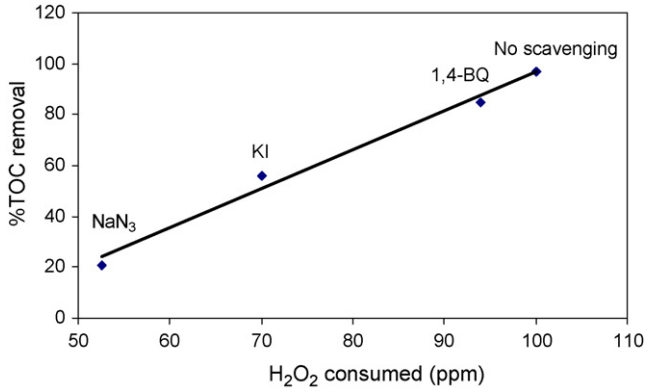

Fig. 9. Relation between %TOC removal and H_2O_2 consumed in the presence of free-radical-scavenging agents, artificial UV-A/C system. Experimental conditions: $[H_2O_2] = 100\ mg\ L^{-1}$; $[Fe(II)] = 2\ mg\ L^{-1}$; $[H_2C_2O_4] = 60\ mg\ L^{-1}$; pH = 4; $[PA] = 20\ mg\ L^{-1}$.

at equilibrium according to Eq. (17), which is favored by reaction between $HO_2^{\bullet}$ and ferrioxalate according to Eq. (24):

$$HO_2^{\bullet} + Fe(III)(C_2O_4)_3^{3-} \rightarrow Fe(II) + H^+ + O_2 + 3C_2O_4^{2-} \quad (24)$$

However, the role of these species was different with the solar radiation source, as shown in Fig. 8b. In this case, superoxide and hydroxyl radicals were the main species contributing to the mineralization of PA solutions. The most significant role of $O_2^{\bullet -}$ was due to its higher generation by Eq. (23), as, with solar light, the ferrioxalate photochemistry is more active because the generated $CO_2^{\bullet -}$ concentration is higher.

Fig. 9 illustrates the relation between the %TOC removal reached (in the presence of radical quenchers) and the amount of H_2O_2 consumed. As seen here, the mineralization degree was proportional to the hydrogen peroxide consumed during the reaction, and it was independent of the type of radicals present in the reaction medium. Iron, in this system, is cycled between the +2 and +3 oxidation states according to Eqs. (10) to (13). Fe(III) can be generated by the Fenton reaction (Eq. (5)). However, the oxidation of PA involves the generation of reducing species capable of transforming Fe(III) into Fe(II), as previously reported [11], so Fe(II) is not depleted, and different free-radical production is limited only by the availability of light and H_2O_2.

4. Conclusions

Protocatechuic acid solutions can be efficiently photodegraded (96–97% TOC removal) using the ferrioxalate-assisted artificial UV-A/C or solar photo-Fenton systems, but with different optimum operating conditions. When artificial UV light was used in the presence oxalic acid, the degradation rate was higher in the UV-C system than in the UV-A system as ferrioxalate complexes were first formed at 200–280 nm. The pH and oxalic acid-addition parameters in the solar process could increase the reaction rate or cause inhibition effects depending on the operating conditions. H_2O_2 addition positively affected the rate up to an optimal concentration, but when H_2O_2 was in excess the degradation rate decreased, as it may act as hydroxyl radical scavenger. The optimal pH was near 4, where the regeneration of Fe(II) by ferrioxalate photolysis and generation of extra hydroxyl radicals was faster. $^{\bullet}OH$ radicals were the main oxidative species in the artificial UV-A/C process while superoxide and $^{\bullet}OH$ radicals played the most significant roles in the solar process. Artificial UV-A/C light can be used as an alternative to solar CPC on cloudy days.

Acknowledgements

Financial support from the Consejería de Educación y Ciencia of the Junta de Comunidades de Castilla-La Mancha (PCI08-0047-4810) is gratefully acknowledged.

References

[1] M. Rodríguez, S. Malato, C. Pulgarín, S. Contreras, D. Curcó, J. Giménez, S. Esplugas, Solar Energy 79 (2005) 360–368.
[2] R.F.P. Nogueira, M.R.A. Silva, A.G. Trovó, Solar Energy 79 (2005) 384–392.
[3] A. Durán, J.M. Monteagudo, E. Amores, Appl. Catal. B: Environ. 80 (2008) 42–50.
[4] S. Malato, J. Blanco, J. Cáceres, A.R. Fernández-Alba, A. Agüera, A. Rodríguez, Catal. Today 76 (2002) 209–220.
[5] H. Yao-Hui, T. Shu-Ting, H. Yi-Fong, C. Chuh-Yung, J. Hazard. Mater. 140 (2007) 382–388.
[6] C. Yong, W. Feng, L. Yixin, D. Nansheng, B. Nikolai, G. Evgeni, J. Hazard. Mater. 148 (2007) 360–365.
[7] J.M. Monteagudo, A. Durán, I. San Martin, M. Aguirre, Appl. Catal. B: Environ. 89 (2009) 510–518.
[8] Y. Lee, J. Jeong, C. Lee, S. Kim, J. Yoon, Chemosphere 51 (2003) 901–912.
[9] J. Jeong, J. Yoon, Water Res. 38 (2004) 3531–3540.
[10] Y. Chen, F. Wu, Y. Lin, N. Deng, N. Bazhin, E. Glebov, J. Hazard. Mater. 148 (2007) 360–365.
[11] F.J. Rivas, J. Frades, M.A. Alonso, C. Montoya, J.M. Monteagudo, J. Agric. Food Chem. 53 (2005) 10097–10104.
[12] W. Gernjak, T. Krutzler, A. Glaser, S. Malato, J. Caceres, R. Bauer, A.R. Fernández-Alba, Chemosphere 50 (2003) 71–78.
[13] F.J. Benitez, J. Beltran-Heredia, J.L. Acero, T. González, Water Res. 30 (1996) 1597–1604.
[14] G.E.P. Box, W.G. Hunter, J.S. Hunter, Statistics for Experimenters: An Introduction to Design, Data Analysis and Model Building, Ed. Wiley, New York, 1978.
[15] D.P. Morgan, C.L. Scofield, Neural Networks and Speech Processing, Kluwver Academic Publishers, London, 1991.
[16] R. Nath, B. Rajagopalan, R. Ryker, Comput. Oper. Res. 24 (1997) 767–773.
[17] D.W. Marquardt, J. Soc. Ind. Appl. Math. 11 (1963) 431–441.
[18] K.A. Hislop, J.R. Bolton, Environ. Sci. Technol. 33 (1999) 3119–3126.
[19] A. Aris, P.N. Sharrat, Environ. Technol. 27 (2006) 1153–1161.
[20] W. Li, S. Zhao, B. Qi, Y. Dua, X. Wang, M. Huo, Appl. Catal. B: Environ. 92 (2009) 333–340.
[21] S. Malhotra, M. Pandit, J.C. Kapoor, D.K. Tyagi, J. Chem. Technol. Biotechnol. 80 (2005) 13–19.